Journal of Computational and Applied Mathematics 476 (2026) 117094

Contents lists available at ScienceDirect

Journal of Computational and Applied Mathematics

journal homepage: www.elsevier.com/locate/cam

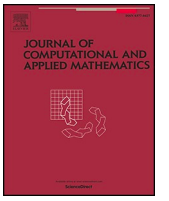

Optimizing thin-layer solar drying of green peas with zeolite under challenging environmental conditions

Melike Sultan Karasu Asnaz

Department of Industrial Engineering, Balikesir University, Balikesir, Turkey

ARTICLE INFO

Keywords:
Solar drying
Thin-layer drying
Drying kinetics
Genetic algorithm
Model optimization
Vegetable dehydration
Clinoptilolite zeolite
Renewable energy in agriculture

ABSTRACT

Solar drying is a sustainable technique for food preservation, but its efficiency drops significantly under low solar radiation and high humidity conditions. This study addresses this challenge by integrating clinoptilolite zeolite as a passive moisture adsorbent into a thin-layer solar dryer and evaluating its effect on green pea drying performance under suboptimal spring conditions in Balıkesir, Turkey. Two experimental trials, conventional and zeolite-enhanced, were conducted on consecutive days with closely matched weather profiles.

The results show that zeolite integration shortened total drying time by 7.1 % (from 7.0 to 6.5 hours) and increased the peak drying rate by 42 %. A 15 % reduction in chamber relative humidity was observed, along with improved energy metrics: 4.6 % lower specific energy consumption (SEC) and 5.4 % higher specific moisture extraction rate (SMER). Six thin-layer drying models were evaluated using genetic algorithm optimization. Among them, the proposed four-parameter Karasu model outperformed others, achieving $R^2 = 0.9968$ and RMSE = 0.0174. Sensitivity analysis identified the shape parameter (n) as the most influential. Zeolite moisture uptake followed a logarithmic trend, reaching 92.6 g (18.5 g/kg). The results confirm that zeolite effectively improves drying kinetics and humidity control under challenging conditions. The Karasu model provides a reliable tool for predicting drying behavior in solar drying systems.

1. Introduction

1.1. Background

As world concerns about climate change and energy sustainability issues grow, the agricultural sector is seeking to adopt environmentally friendly practices across all production stages. Drying is a critical food preservation method that represents a post-harvest process consuming substantial energy and contributing to greenhouse gas emissions. Solar drying has emerged as a promising sustainable alternative, harnessing renewable energy to reduce both environmental impact and operational costs while maintaining food quality and safety [1]. However, the effectiveness of solar drying systems is heavily dependent on environmental conditions, which can significantly limit their application in regions with suboptimal weather patterns.

Drying is fundamentally a moisture removal process that reduces water activity in agricultural products, thereby controlling microbial growth, enzymatic reactions, and chemical deterioration [2]. This preservation technique simplifies handling, reduces transportation costs, and extends shelf life. However, conventional drying methods rely predominantly on fossil fuels with significant energy consumption and environmental impact [3]. Solar drying offers a sustainable alternative, but faces challenges related to

E-mail address: karasu@balikesir.edu.tr.

https://doi.org/10.1016/j.cam.2025.117094
Received 29 April 2025; Received in revised form 5 September 2025;
Available online 19 September 2025

Nomenclature

MC	Moisture content
M_t	Moisture content at time t
M_e	The equilibrium moisture content
M_o	The initial moisture content
MR	The moisture ratio
DR	Drying rate in % d.b./h
δR	Total uncertainties
R_{MR}	Uncertainty for moisture ratio
R_{DR}	Uncertainty for drying rate
GA	Genetic algorithm
RMSE	Root mean square error
R^2	Coefficient of determination
SMER	Specific moisture extraction rate
SEC	Specific energy consumption
S_i	Sensitivity indices
$S_{i,normalized}$	Normalized sensitivity indices
RH	Relative humidity
w.b.	wet basis
d.b.	dry basis

intermittent energy supply, weather dependence, and varying efficiency under different climatic conditions.

1.2. Problem statement

However, performance of solar drying systems is significantly hampered under challenging environmental conditions, particularly during periods of low solar irradiance and high ambient humidity. These conditions are common in many agricultural regions during spring and autumn months, precisely when post-harvest processing is often necessary. The inconsistent drying rates under such conditions can lead to extended drying times, increased energy consumption, and potential quality degradation of agricultural products.

The limitations of solar drying under low irradiance and high humidity conditions have direct economic, environmental, and social implications. Economically, prolonged drying times and inconsistent performance increase post-harvest losses and energy costs, particularly for small-scale producers lacking access to controlled environments [4]. Environmentally, compensating for poor solar drying with auxiliary heating systems often increases fossil fuel usage, and CO_2 emissions [5]. Inefficient drying during unfavorable weather conditions poses a risk to food quality and safety. This issue is particularly critical in rural areas, where affordable preservation methods are vital, as it worsens food insecurity [6]. By addressing these challenges with passive humidity control by integration of moisture-adsorbing materials like zeolite, this study proposes a sustainable enhancement to solar drying that aligns with energy-access and food-security priorities.

While zeolite presents a promising solution to improve solar drying efficiency under suboptimal weather conditions, it is not without limitations. Natural zeolites may contain heavy metals or impurities, and pose potential contamination risks if not properly treat [7,8]. Furthermore, zeolite requires periodic regeneration through thermal desorption at elevated temperatures which may introduce additional energy costs [3]. These factors must be carefully considered in large-scale implementations to ensure both food safety and energy sustainability. Despite these constraints, this study explores the feasibility of zeolite as a passive enhancement strategy requiring no external energy input during drying operation itself.

1.3. Research objectives

This study aims to:

1. Evaluate the effectiveness of clinoptilolite zeolite in enhancing solar drying of green peas under unfavorable weather conditions characterized by low solar irradiance and high humidity.
2. Quantify the improvement in drying kinetics and reduction in drying time achieved through zeolite integration.
3. Develop and validate mathematical models that accurately describe the thin-layer drying behavior of green peas
4. Conduct sensitivity analysis to identify the most influential parameters affecting the drying process and model accuracy.
5. Measure the moisture absorption capacity of zeolite under solar drying conditions to understand its practical efficacy.

This research addresses several critical gaps in the current understanding of zeolite-enhanced solar drying. First, it provides empirical evidence of zeolite effectiveness under suboptimal weather conditions that are rarely examined in controlled laboratory

studies. Second, it offers a comprehensive mathematical modeling approach using genetic algorithm optimization, which enhances the predictability of drying behavior in zeolite-enhanced systems. Third, the sensitivity analysis presented in this study constitutes a novel contribution that explains the relative importance of various model parameters which could be helpful for future design.

1.4. Paper organization

The remainder of this paper is organized as follows: In Section 2, the current state of research on solar drying technologies, focusing on the application of zeolite and other sorption materials, and the mathematical modeling approaches used to describe drying kinetics are explored. Section 3 describes the materials, experimental setup, and methods employed. Section 4 provides results related to environmental measurements, drying kinetics, and modeling performance. Section 5 discusses practical implications, zeolite performance, and modeling validation. Finally, Section 6 concludes the study by summarizing the key findings and suggesting directions for future research.

2. Literature review

Recent advancements in solar drying technology have focused on addressing the inherent limitations of conventional designs, particularly regarding efficiency, reliability, and performance under variable weather conditions. Nnamchi et al. [1] provided a comprehensive review of solar drying mechanisms, highlighting the evolution from passive systems to more sophisticated hybrid designs that incorporate auxiliary energy sources and smart control systems. Their analysis emphasized the growing trend toward sustainability metrics in evaluating drying systems, including energy efficiency ratios, carbon footprint assessments, and life-cycle analyses. Kherrafi et al. [2] examined recent innovations in solar dryer designs, noting significant improvements in thermal efficiency through the integration of heat storage materials and optimized airflow configurations. Their study demonstrated that advanced collector designs with selective absorber coatings could achieve temperature gains 15-20 % higher than conventional flat-plate collectors, even under moderate solar radiation conditions.

The application of desiccant and sorption materials in drying systems represents a promising approach to overcome the limitations of traditional solar drying methods. Dake et al. [3] conducted a comprehensive review of sorption materials in solar dryers, identifying their dual functionality as dehumidifiers and thermal energy storage media. Their analysis highlighted how sorption-enhanced systems could maintain continuous drying operations through a regenerative cycle, where daytime solar energy drives desorption to regenerate the material, while nighttime operation utilizes the stored energy through exothermic heat release.

Zeolite-based solar drying has demonstrated considerable advantages across multiple agricultural products, as evidenced by several key studies in the field. Ying et al. [9] investigated zeolite-based drying for paddy rice, demonstrating that zeolites could significantly enhance drying efficiency while preserving product quality. The study reported energy savings of approximately 25 % compared to conventional hot-air drying methods, with superior product quality indicators including reduced cracking and improved whiteness. The relationship between zeolite weight and drying performance was investigated by Siqhny et al. [10] and they found that increasing zeolite weight led to enhanced moisture reduction and thermal efficiency when drying moringa leaves. For cereal crops, Utari et al. [11] demonstrated that zeolite adsorption techniques applied to paddy rice at temperatures between 40-60 °C resulted in a 19 % higher constant drying rate compared to conventional methods. Buchori et al. [12] established that applying a 1:3 zeolite ratio at 40-50 °C for corn drying reduced processing time by an hour while simultaneously improving energy efficiency to 81.23 %. Collectively, these findings highlight the substantial potential of zeolite integration in solar drying systems to enhance both drying efficiency and final product quality across diverse agricultural commodities.

Mathematical modeling plays a crucial role in understanding, predicting, and optimizing drying processes. Recent studies have compared various thin-layer mathematical models for solar drying across different food materials and conditions. Metwally et al. [13] evaluated 12 models for date fruits, finding the Two-term and Modified Page III models best for open-air drying, while Two-term Exponential and Newton models performed well for automated solar drying. Haydary et al. [14] developed a process conditions sensitive model for hot air convective drying, applicable across a range of temperatures, air velocities, and humidity levels. Sherazi et al. [15] examined five models for drying peaches and wild mint, emphasizing the impact of mass flow rate on model coefficients. Abdelkader et al. [16] applied ten drying kinetics models to sweet potato drying, with the Page model showing the best fit. These studies demonstrate that model performance varies depending on the specific food material and drying conditions, highlighting the importance of selecting appropriate models for accurate predictions.

Peter et al. [17] investigated the application of computational intelligence techniques, particularly thin-layer models, Artificial Neural Networks (ANN), Support Vector Machines (SVM), k-Nearest Neighbors (kNN) for estimation in drying kinetics. This paper recommends using computational intelligence modeling, particularly the standardized Pearson universal kernel, for accurately modeling the drying kinetics. Wang et al. [18] utilizes machine learning models to predict its operational performance (temperature, humidity, and power generation), and concluded that the Convolutional Neural Network (CNN) model demonstrating the highest accuracy in predicting system parameters. Similarly, genetic algorithm has been effectively employed to validate and optimize nonlinear regression-based mathematical models in other energy-related applications as in [19] that proposed a genetic algorithm supported model for hospital pneumatic systems, achieving up to 43 % improvement in energy efficiency.

The effectiveness of solar drying systems is significantly influenced by environmental factors, particularly solar radiation intensity, ambient temperature, relative humidity, and wind speed. Understanding these influences is crucial for designing efficient and reliable solar drying systems. Zoukit et al. [20] examined the impact of daily temperature variations on the drying kinetics of agricultural products in solar greenhouse dryers. Their findings demonstrated that temperature fluctuations, particularly the significant drop

during nighttime, could extend drying times by 30-40 % compared to constant-temperature controlled environments. This highlighted the importance of thermal storage systems or auxiliary heating sources to maintain consistent drying rates. Beigi et al. [21] investigated the relationship between airflow rates and drying efficiency in forced convection solar dryers. Their parametric study identified optimal airflow velocities for different product types and loading densities, demonstrating that excessive airflow could actually reduce drying efficiency by lowering the drying air temperature, while insufficient airflow limited the moisture-carrying capacity of the system.

The reviewed literature reveals a limited evaluation of zeolite effectiveness in solar drying under low solar irradiance and high humidity conditions. So, this study aims to address this gap by providing empirical evidence of zeolite performance under suboptimal conditions and developing robust mathematical models to predict the drying behavior in zeolite-enhanced solar drying systems.

3. Materials and methods

3.1. Experimental setup

The solar drying experiments were conducted in Balıkesir, Turkey (39.7° N, 27.9° E, 148 m altitude), using a forced/natural convection hybrid solar dryer fabricated from stainless steel as seen Fig. 1. The system was thermally optimized with 60 mm glass wool to minimize heat losses and coated with high-absorptivity matte black paint to enhance solar energy capture.

A dual-mode airflow system was designed to operate under both forced and natural convection. Two 24 V DC fans (0.25 A each) were integrated at the collector inlet. And an aspirator-type rotating chimney cowl was mounted to exploit wind-driven draft. This solar dryer's design parameters shown in Table 1 are fully detailed and explained in Karasu Asnaz and Dolcek 's [22] study.

In Balıkesir, the conditions in April presented significant challenges for solar drying, with a solar irradiance of 458 W/m^2, approximately 50.4 % lower than the peak summer value of 689 W/m^2 observed in July. Additionally, the average temperature in April was 12.4 °C, which nearly doubled to 25.9 °C in July, further limiting thermal energy availability. The higher relative humidity of 68 % in April, compared to 53 % in July, challenging moisture retention and drying efficiency [23].

These unfavorable conditions, particularly the lower solar irradiance and higher relative humidity, make April a-less-than-ideal period for evaluating the effectiveness of solar drying systems. Consequently, the primary objective of our experiments is to demonstrate the feasibility of enhancing solar drying efficiency in environments and during periods characterized by high humidity through the integration of desiccants such as zeolite.

3.2. Materials

3.2.1. Green peas

Freshly harvested green peas (*var. Pisum sativum L.*) were provided by a local farmer in Balikesir. Samples weighing 150 g were obtained for each experiment and kept in plastic bags at 4 °C until the drying process. Before drying, samples were sorted to remove any damaged peas, thoroughly washed under running water, and drained.

Before solar drying, green peas were blanched (90 °C, 2-3 min) to inactivate enzymes and accelerate moisture removal, then dipped in 0.5 % citric acid to prevent browning and preserve color. This multi-pretreatment process improved drying efficiency while

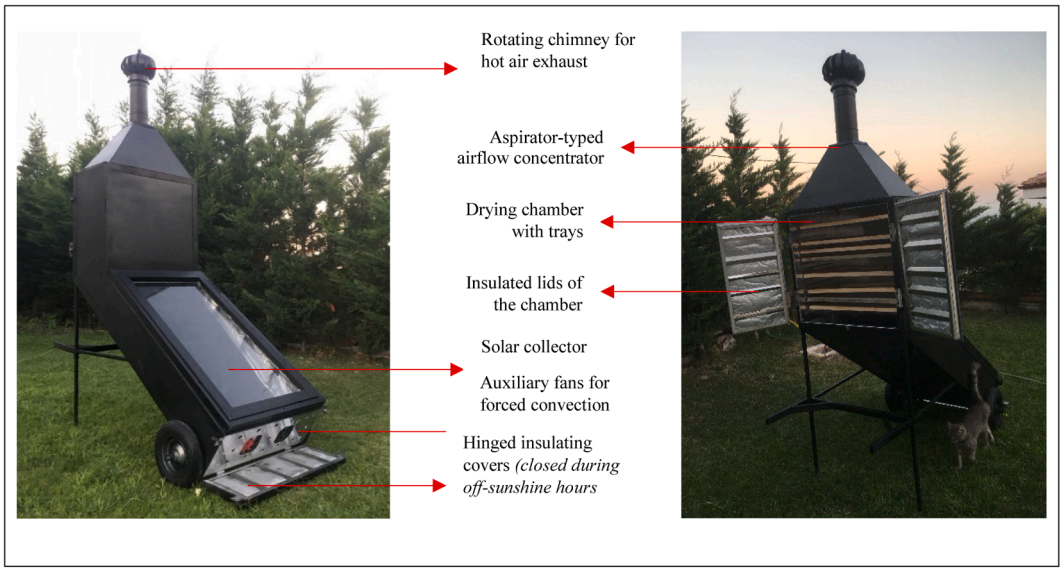

Fig. 1. Front (left) and rear (right) views of the solar dryer.

Table 1
Technical specifications of the solar dryer.

Component	Specifications
Body Material	2 mm thick stainless steel, painted matte black
Insulation	60 mm glass wool (entire system)
Solar Collector	- Dimensions: 80 cm × 160 cm - Absorber: 10-layer blackened perforated metal flyscreen (aperture ratio: 0.6) - Glazing: 6 mm tempered glass, 39° tilt angle
Drying Chamber	- Dimensions: 30 cm × 70 cm × 80 cm - Capacity: 11 stainless steel wire mesh trays (0.5 mm mesh size) - Experimental setup: The upper tray for product (boundary-layer isolation), the bottom tray for the zeolite

maintaining product quality, as indicated in previous studies [6,8,24].

Following blanching and acid treatment, peas were immediately soaked in an ice water bath for 30 seconds to stop the cooking process, then drained thoroughly. Excess water was removed using a muslin cloth. Drying trays were prepared by spreading the green peas uniformly in a single layer, ensuring no overlap between individual peas.

The initial moisture content of blanched samples was determined by drying a representative sample in an electric drying oven at 105 °C for 24 h and found to be 77 % on wet basis (w.b.). The drying process was carried out until a constant weight was observed, and the target equilibrium moisture content of dried green peas was set at 10.37 % w.b.. Products with moisture content exceeding this target level are susceptible to mold growth, which would compromise the quality of the finished product.

3.2.2. Zeolite

Zeolites are crystalline aluminosilicate minerals with a three-dimensional framework structure containing uniformly sized pores and channels that allow selective adsorption of water molecules [9]. Natural zeolites are abundant, cost-effective, and environmentally friendly, making them particularly suitable for agricultural applications. Their high surface area and porosity enable substantial moisture adsorption capacity, with some zeolite varieties capable of absorbing 0.12-0.14 kg of water per kg of material [8].

In solar drying systems, zeolite absorbs moisture from the air, reducing the relative humidity and enhancing the driving force for drying. This process not only accelerates drying rates but also improves the uniformity of moisture removal [10,25,26]. In this study, untreated clinoptilolite zeolite particles in the 1–3 mm size range were used, as this variety is locally available in the region. Besides, smaller particle sizes offer a larger specific surface area, facilitating greater contact with moisture and enhancing adsorption efficiency. Prior to the experiment, a drying process at 105 °C for 12 h under laboratory conditions until a constant weight was achieved, ensuring the removal of any initial moisture.

3.2.3. Experimental procedure

The control experiment was conducted on 15 April 2024 at 09:00 using 150 g of green peas evenly distributed on trays equipped with three load cells. Weight data were recorded at 30-min intervals on an SD card, The drying process was carried out until a constant weight was observed.

In the experimental setup, 5 kg of clinoptilolite zeolite (1–3 mm) was placed at the dryer's air inlet (lower tray), while the green pea sample (150 g) was positioned in upper tray. This arrangement prioritized dehumidification of incoming air, as the zeolite adsorbed moisture before the air reached the product, directly lowering the relative humidity and leveraging the exothermic heat of adsorption to warm the airflow that leads to accelerate evaporation. This design aligns with Dake et al.'s [3] study that emphasizes sorbent placement at dryer inlets for maximal humidity control, and ensures efficient use of adsorption heat to supplement solar energy. Both

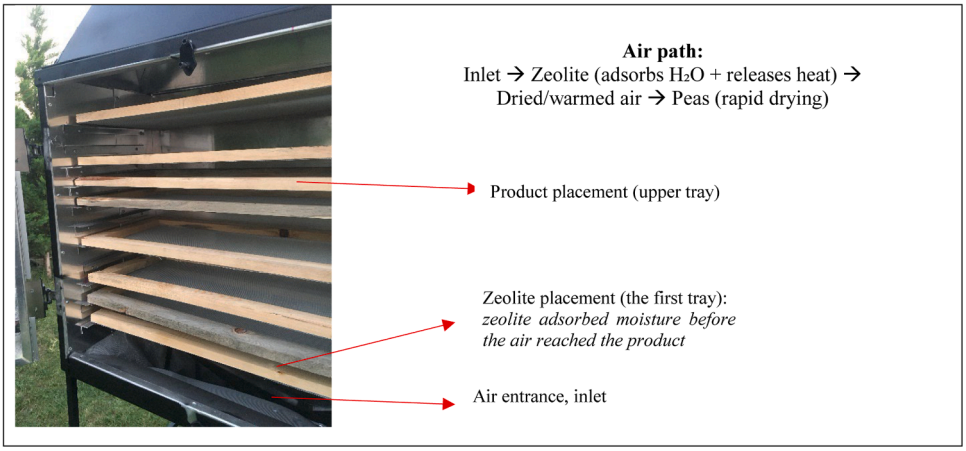

Fig. 2. Experimental setup: airflow direction and placement of zeolite and peas in the drying chamber.

sample and zeolite weights were monitored using load cells (Fig. 2).

Due to the meteorological constraints, the experiments were conducted on two consecutive days (April 15 and 16) that exhibited very similar weather conditions. This approach was necessary since the study's objective was to evaluate zeolite performance under low solar irradiance and high humidity conditions typical of early spring in Balıkesir. Beyond this narrow weather window, environmental conditions began shifting toward summer patterns, which would have introduced confounding variables. Therefore, while multiple runs were performed during setup and calibration, only two representative experimental trials – one control and one zeolite-enhanced – were selected for detailed comparison under closely matched conditions.

4. Measurement and analysis

4.1. Environmental parameters

To accurately assess the drying kinetics and the impact of zeolite integration, key environmental and operational parameters were meticulously monitored throughout both the control (15th April) and zeolite-enhanced (16th April) experiments. Monitoring these environmental parameters is crucial as they significantly influence the drying kinetics and overall efficiency of solar drying systems. These parameters included solar irradiance, ambient conditions (temperature and relative humidity), internal dryer temperatures (collector outlet and drying chamber), drying chamber relative humidity, and airflow rate.

Solar irradiance is the primary driver of thermal energy input in solar dryers and directly affects the temperature rise within the system. Variations in solar radiation can lead to significant differences in drying time and efficiency [20].The experiments were conducted on two consecutive days selected for their meteorological similarity to ensure a valid comparison between the drying methods. Fig. 3 illustrates the solar radiation variation recorded during the two experimental days: 15th April (control experiment) and 16th April (zeolite-enhanced experiment). These graphs display the full-day solar radiation profile and the specific experimental hours for each day. The experimental drying periods were from 09:00-16:00 on 15th April and 09:00-15:30 on 16th April. During these durations, the average solar radiation was recorded 946.18 W/m^2 for 15th April and 973.11 W/m^2 for 16th April. The average solar radiation over the entire day for these days was 541.85 W/m^2 and 544.03 W/m^2, respectively. While the average monthly solar radiation in April is 458 W/m^2, the experimental days experienced higher values due to clear sky and minimal cloud coverage.

Table 2 summarizes the environmental and operational parameters of those experiment days.

Internal dryer conditions were monitored using sensors placed at the solar collector outlet and within the drying chamber. The average collector outlet temperature, representing the temperature of the air entering the drying chamber, was slightly higher during the zeolite experiment (59.5 °C) compared to the control (58.2 °C). The collector outlet temperature governs the initial thermal potential of the air entering the chamber, influencing both the drying rate and moisture removal efficiency [21]. Consequently, the average drying chamber temperature was also marginally higher in the zeolite experiment (43.84 °C vs. 42.77 °C). A notable difference was observed in the average drying chamber relative humidity, which was lower during the zeolite-enhanced experiment (25.98 %) compared to the control experiment (28.71 %), as detailed in Table 2. This reduction is attributed to the dehumidifying action of the zeolite placed in the second experiment. Relative humidity within the drying chamber is a critical parameter affecting the vapor pressure gradient between the product surface and the drying air. Lower RH increases the drying potential and enhances mass transfer rates [10].

The average airflow rate was consistent across both experiments at 0.3 m/s by the help of two fans, ensuring that differences in drying performance were primarily due to the presence of the zeolite rather than other variations Airflow controls the removal of saturated air and the delivery of fresh drying air, thus directly impacting drying kinetics and uniformity [5].

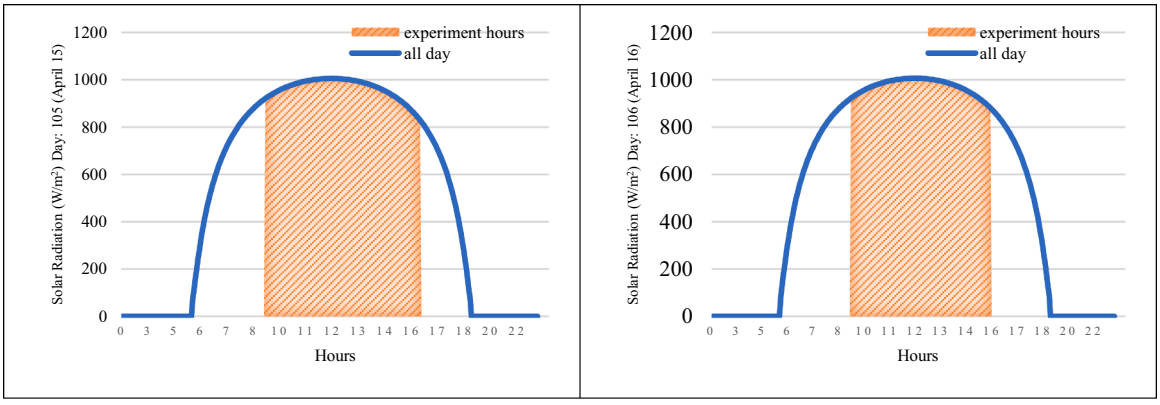

Fig. 3. Solar radiation variation throughout the experiment days.

Table 2
Summary of average environmental and operational parameters.

Parameter	Unit	Control Experiment (15th April)	Zeolite-Enhanced Experiment (16th April)
Av. Daily Solar Radiation	W/m²	541.85	544.03
Av. Solar Radiation During Drying Hours	W/m²	946.18	973.11
Max. Solar Radiation	W/m²	1006	1007
Av. Ambient Temperature	°C	12.9	13.0
Av. Ambient Rel. Humidity	%	38.3	36.6
Av. Collector Temperature	°C	58.2	59.5
Av. Chamber Temperature	°C	42.77	43.84
Av. Chamber Rel. Humidity	%	28.71	25.98
Av. Airflow Rate	m/s	0.3	0.3

4.2. Data collection, uncertainty and sensitivity analysis

An Arduino-based system recorded parameters for 30-min intervals including: i. Thermal data (*chamber/collector/ambient temperature (±0.5 °C) and humidity (±2–3 % RH) via Testo 174H and DHT22 sensors*) and ii. Mass data (*sample weight (±0.2 g) using 1 kg load cells*). Total uncertainties were quantified via root mean square error with key independent variables and their contributions summarized in Table 3, detailed explanations can be found in [27] (Fig. 4).

The overall uncertainty (δR) of any calculated parameter $R(x_1, x_2, \ldots, x_n)$ dependent on measured variables x_i with individual uncertainties δx_i was determined using error propagation theory by Eq. (1):

$$R = \left\{ \left(\frac{\partial R}{\partial x_1} \delta x_1 \right)^2 + \left(\frac{\partial R}{\partial x_2} \delta x_2 \right)^2 + \ldots + \left(\frac{\partial R}{\partial x_n} \delta x_n \right)^2 \right\}^{\frac{1}{2}} \tag{1}$$

The moisture ratio ($MR = M_t/M_0$) uncertainty (R_{MR}) accounts for errors in initial (M_0) and equilibrium (M_e) moisture measurements as calculated in Eq. (2):

$$R_{MR} = \left\{ \left(\frac{\partial MR}{\partial M_e} \delta R_{M_e} \right)^2 + \left(\frac{\partial MR}{\partial M_0} \delta R_{M_0} \right)^2 \right\}^{\frac{1}{2}} \tag{2}$$

The drying rate ($DR = \Delta M/\Delta t$) uncertainty (R_{DR}) incorporates mass (M_t, $M_{t+\Delta t}$) and temporal (Δt) measurement errors and calculated by Eq. (3):

$$R_{DR} = \left\{ \left(\frac{\partial DR}{\partial M_t} \delta R_{M_t} \right)^2 + \left(\frac{\partial DR}{\partial M_{t+\Delta t}} \delta R_{M_{t+\Delta t}} \right)^2 + \left(\frac{\partial DR}{\partial \Delta t} \delta R_{\Delta t} \right)^2 \right\}^{\frac{1}{2}} \tag{3}$$

To quantify the relative influence of measurement errors on key outputs, a local sensitivity analysis was performed by varying input parameters (±δR) while monitoring changes in MR and DR. Sensitivity coefficients were calculated by perturbing each input parameter by its experimental uncertainty (±δR) and normalizing the output response of moisture ratio and drying rate, as follows in Eq. (4):

$$S_i = \frac{\left(\frac{\Delta Output}{Output} \right)}{\left(\frac{\Delta Input}{Input} \right)} \tag{4}$$

where $\Delta Output$ is the change in MR or DR due to $\Delta Input$. Now, to compare the relative influence of parameters, absolute sensitivity indices (S_i) were converted to normalized values summing to unity by Eq. (5):

$$S_{i,normalized} = \frac{S_i}{\sum_{j=1}^{n} S_j} \tag{5}$$

Both Table 4 and Fig. 5 show the key factors affecting solar drying performance. Table 5 summarizes the sensitivities for solar drying kinetics. As can be seen, mass measurement accuracy has the greatest impact on MR prediction ($S_{i,normalized}$ = 82 %), emphasizing the need for precise load cell calibration. Temperature changes are strongly linked to DR ($S_{i,normalized}$ = 61 %), as

Table 3
Instruments used for the data collection.

Parameter	Instrument	Accuracy	Key Independent Variables (δR)
Temperature	Testo 174H	±0.5 °C	Sensor calibration (±0.35)
Relative humidity	DHT22	±2–3 % RH	Hygrometer drift (±0.10)
Mass loss	Load cells	±0.2 g	Tray friction (±0.269)

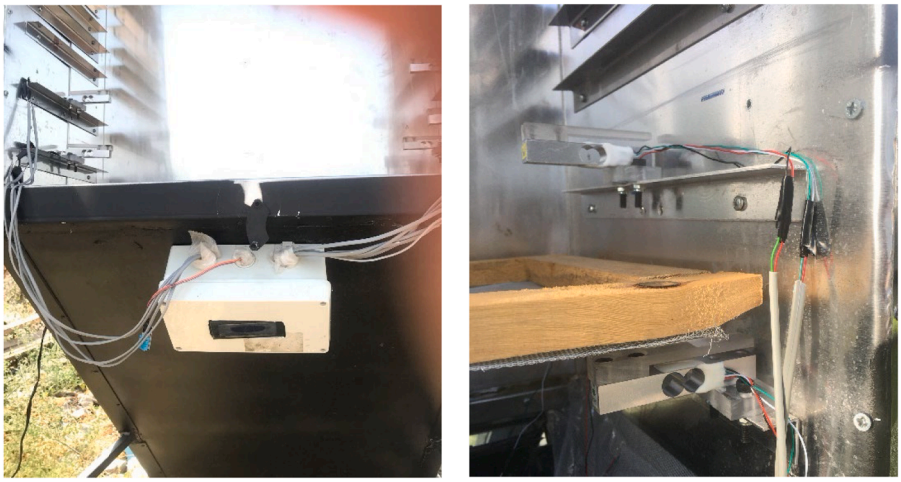

Fig. 4. (a) Data acquisition system for monitoring solar dryer parameters (b) Placement of load cells on drying trays for real-time weight measurement.

Table 4
Independent variables for R analysis.

Parameter	Instrument	Accuracy	Dominant Uncertainty (δR)
Temperature	Testo 174H	±0.5 °C	Sensor calibration (0.35)
Mass loss	Load cells	±0.2 g	Tray friction (0.269)
Time interval	Arduino clock	±0.1 min	Data logging delay (0.10)

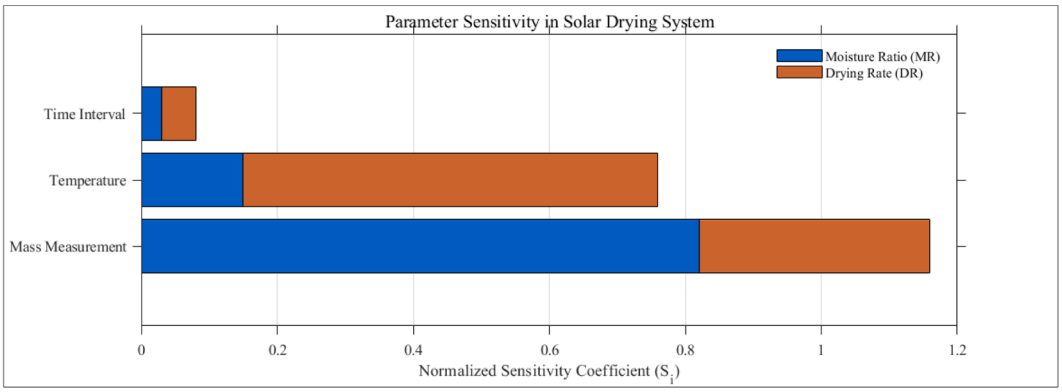

Fig. 5. Parameter sensitivity in solar drying.

Table 5
Sensitivities for solar drying kinetics.

	Sensitivity for Moisture Ratio		Sensitivity for Drying Rate	
Parameter	Raw S_i	$S_{i,normalized}$	Raw S_i	$S_{i,normalized}$
Mass	**3.72**	**0.82***	1.54	0.34
Temperature	0.68	0.15	**2.76**	**0.61***
Time	0.14	0.03	0.23	0.05
Sum	4.54	1.00	4.53	1.00

temperature influences vapor pressure. The low sensitivity to time intervals ($S_{i,normalized} < 5$ %) confirms that 30 min data logging is adequate. These findings show that controlling mass and temperature is essential for accurate thin-layer drying in zeolite-enhanced systems.

4.3. Drying kinetics

The moisture ratio (MR), a dimensionless parameter, was calculated as Eq. (6):

$$MR = \frac{(M_t - M_e)}{(M_0 - M_e)} \tag{6}$$

where M_t is the moisture content at time t, M_0 is the initial moisture content, and M_e is the equilibrium moisture content. However, since M_e is often negligible in forced-convection drying systems, MR was simplified to M_t/M_0 for practical analysis [4].

The drying rate (DR, % d.b./h) was determined from the temporal moisture loss by Eq. (7):

$$DR = \frac{dM}{dt} \approx \frac{M_{t+\Delta t} - M_t}{\Delta t} \tag{7}$$

where Δt is the time increment between measurements. DR quantifies the evaporation intensity which is an important indicator for evaluating drying efficiency.

Drying kinetics models listed in Table 6 were then applied to describe the MR-time relationship, with parameters optimized using genetic algorithms.

To assess energy utilization of the solar drying system Specific Moisture Extraction Rate (SMER), and Specific Energy Consumption (SEC) which are critical for quantifying system performance and enabling comparative analysis, were evaluated. The amount and type of energy supplied (e.g., electrical, thermal) play a crucial role in determining the efficiency of moisture extraction [28].

SMER is the amount of moisture extracted per unit of energy input, and calculated using Eq. (8):

$$SMER = \frac{m_{evap}}{E_{supplied}} = \frac{m_{evap}}{E_{solar} + E_{fan}} \tag{8}$$

Here, $E_{supplied}$ is the total energy supplied to the dryer (kWh), consisting of solar energy in kWh (E_{solar}) that is the incident solar radiation captured by the collector calculated as Eq. (9), and fan energy in kWh (E_{fan}) that is the electrical energy consumed by the airflow system, determined by Eq. (10) [24];

$$E_{solar} = \frac{I \times A \times t}{1000} \tag{9}$$

where I is average solar radiation (W/m^2), A is collector area (1.28 m^2), and t is drying time in hours,

$$E_{fan} = \frac{P_{fan} \times t}{1000} \tag{10}$$

The power consumed by the fans (P_{fan}) was calculated by multiplying the voltage (24 V) and current (0.25A) drawn by each of the two fans, with the total result then converted to kW.

And, m_{evap} is the mass of evaporated water (kg) and calculated by Eq. (11).

$$m_{evap} = m_0 - \left(\frac{m_0 \times (1 - MC_0)}{1 - MC_f}\right) \tag{11}$$

where m_0 is initial product mass (kg), and MC_0, MC_f are initial and final moisture contents (% w.b.), respectively.

SEC indicates the energy cost to evaporate 1 kg of water. This metric measures the energy required to remove a unit mass of moisture from the drying product, calculated by Eq. (12). It directly indicates the energy efficiency, with lower values signifying better performance [24].

$$SEC = \frac{E_{supplied}}{m_{evap}} \tag{12}$$

Table 6
Drying models.

Drying Model	Equation
Lewis Model	$MR = exp(-kt)$
Page Model	$MR = \exp[-(kt)^n]$
Logarithmic Model	$MR = a\,exp(-kt) + c$
Diffusion Approach	$MR = a\,exp(-kt) + (1-a)\,exp(-kbt)$
Midilli Model	$MR = a \exp[-(kt)^n] + bt$
Karasu Model	$MR = a \exp[-(kt)^n] + c$

4.4. Mathematical modelling

Mathematical modeling plays a crucial role in understanding, predicting, and optimizing drying processes by describing the complex heat and mass transfer phenomena involved. These models provide valuable tools for system design, process control, and performance evaluation, reducing the need for extensive experimental testing [29].

For agricultural products with complex structure and composition, semi-theoretical models often provide a good balance between accuracy and simplicity [27]. These models typically express the MR as a function of drying time and empirical constants that must be determined through experimental data fitting.

In this study, six semi-theoretical thin-layer drying models—Lewis, Page, Logarithmic, Diffusion Approach, Midilli, Karasu—were employed to describe the MR behavior during solar drying. Each model represents a specific mathematical formulation to capture

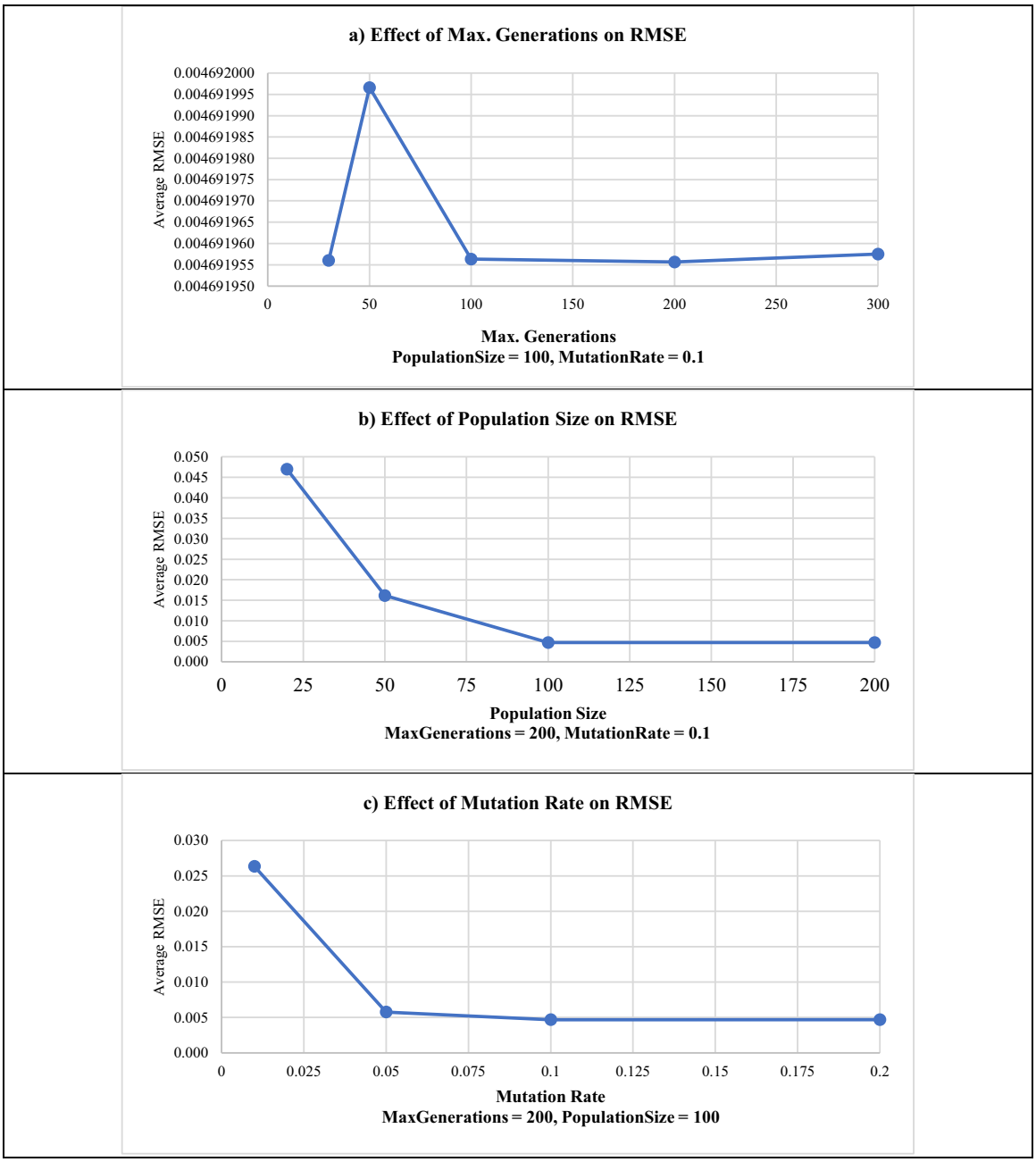

Fig. 6. Effect of GA control parameters on average RMSE: (a) Maximum Generations (fixed PopulationSize = 200, MutationRate = 0.1), (b) Population Size (fixed MaxGenerations = 200, MutationRate = 0.1), (c) Mutation Rate (fixed MaxGenerations = 200, PopulationSize = 100).

drying kinetics, with varying degrees of complexity and flexibility. Genetic Algorithm (GA) optimization was applied to estimate model parameters by minimizing the difference between experimental and predicted MR values. The parameters used in these models have distinct physical interpretations:

- the constant a scales the initial MR, controlling the amplitude of the drying curve;
- k is the drying rate constant, governing how quickly moisture is removed;
- n adjusts the time-dependent curvature of the curve, influencing whether drying accelerates or decelerates;
- c accounts for residual moisture content, enabling better modeling of the final stages of drying by shifting the curve vertically.

These parameters collectively allow each model to simulate different drying behaviors and improve fit accuracy.

The modified version of the Midilli model ($MR = a \exp[-(kt)^n] + bt$) is introduced in [27] as New Model 1 and will be called Karasu model afterwards ($MR = a \exp[-(kt)^n] + c$). Even both models describe MR change during drying, they show critical differences in their physical interpretation and predictive performance. In the Midilli model, parameters a, k and n represent the initial moisture coefficient, drying rate constant, and diffusion exponent, respectively, while the linear term bt accounts for prolonged drying effects. However, this linear term introduces a theoretical limitation. As time (t) progresses, MR can diverge toward unrealistic negative values, violating the physical boundary of equilibrium moisture content.

The Karasu model addresses this limitation by replacing bt with a constant c, which corresponds to the experimentally observable MR_e. This modification ensures asymptotic convergence to a realistic minimum MR value. While this revision eliminates the Midilli model's unphysical divergence to negative MR values at prolonged times, empirical fits of the Karasu model may still yield negative c values that means there may be an overestimation of moisture removal at equilibrium due to experimental artifacts.

Model validation involves comparing predicted values with experimental data using statistical parameters such as coefficient of determination (R^2) as in Eq. 13, root mean square error (RMSE) as in Eq. 14. A higher R^2 value (closer to 1) indicates better correlation between predicted and experimental data, while lower RMSE values suggest better model accuracy [18]. These statistical indicators provide objective criteria for selecting the most appropriate model for a specific drying application [4,30].

$$R^2 = \frac{\sum_{i=1}^{n}\left(MR_i - MR_{pre,i}\right)\cdot\sum_{i=1}^{n}\left(MR_i - MR_{exp,i}\right)}{\sqrt{\sum_{i=1}^{n}\left(MR_i - MR_{pre,i}\right)^2\cdot\sum_{i=1}^{n}\left(MR_i - MR_{exp,i}\right)^2}} \tag{13}$$

$$RMSE = \sqrt{\left[\frac{1}{N}\sum_{i=1}^{N}\left(MR_{pre,i} - MR_{exp,i}\right)^2\right]} \tag{14}$$

4.4.1. Genetic algorithm implementation

In this study, GA was employed for parameter optimization due to its ability to avoid local optima, which is a common issue in fitting complex and nonlinear drying models. Unlike traditional methods that rely on gradients, GA does not require derivative information and can effectively search a wider solution space. This makes it suitable for fitting models with nonlinear parameters such as k, n, and c. As stated by Gulsen et al. [31] GA-based curve fitting is robust to changes in data size, initial parameter ranges, and population structure, making it both reliable and flexible.

The GA was implemented in MATLAB R2021a, to ensure a balance between convergence speed and solution quality, several key parameters were systematically selected. The population size was set to 100 individuals, allowing for sufficient diversity in each generation. The primary termination criterion was a maximum number of 200 generations, based on preliminary convergence behavior. The fitness function was defined as RMSE between the measured and predicted MR values using the models presented in Table 6. The optimization aimed to minimize this error. The configuration and performance of the GA were further assessed through a detailed sensitivity analysis presented in the following section.

4.4.2. Sensitivity analysis of GA parameters

To evaluate the robustness and convergence behavior of the GA, a sensitivity analysis was performed on three key control parameters: maximum number of generations, population size, and mutation rate. For each configuration, the GA was executed five times, and the average RMSE was recorded.

Fig. 6(a) shows the effect of the maximum number of generations on model performance, with the population size and mutation rate fixed at 200 and 0.1, respectively. Varying the maximum number of generations (30, 50, 100, 200, 300) yielded negligible differences in the final RMSE values (average $\approx$ 0.004692) which indicates that convergence typically occurred within the first 100 generations. So, setting MaxGenerations = 200 ensures sufficient convergence while avoiding excessive computation.

Fig. 6(b) shows the influence of population size, with MaxGenerations = 200 and MutationRate = 0.1. Increasing the population (20, 50, 100, 200) showed improved RMSE performance, especially between 20 and 100 individuals. A population size of 100 was found sufficient for the parameter space explored.

Finally, Fig. 6(c) examines mutation rate sensitivity under fixed MaxGenerations = 200 and PopulationSize = 200. Lower mutation rates led to higher RMSE, likely due to premature convergence. Rates of 0.1 or higher produced better and consistent results. This suggests the GA is relatively robust to moderate changes in mutation rate but sensitive to extremely low values.

The computational efficiency of the GA optimization was evaluated by measuring CPU running times across all sensitivity analysis

experiments. Execution times ranged from 0.8 to 2.3 secs, depending on the parameter configuration. Larger population sizes and higher generation numbers required more computation time [32]. Specifically, testing different maximum generations (30, 50, 100, 200, 300) required 0.8–1.6 secs, varying population size (20, 50, 100, 200) needed 0.9–2.3 secs, and mutation rate (0.01, 0.05, 0.10) took the shortest range of 0.8–1.0 s. Convergence occurred well before the maximum generation limit as shown by the rapid stabilization of RMSE values in Fig. 6. All experiments were conducted in MATLAB R2021a on an Intel Core i7 (2.6 GHz), 16 GB RAM system. Finally, the selected GA configuration (PopulationSize = 100, MaxGenerations = 200, MutationRate = 0.1) ran in approximately 1.0 sec and showed strong convergence with low variability, supporting the validity of the optimized model parameters.

5. Results and discussion

5.1. Environmental conditions

Fig. 7 shows the hourly temperature variations for the solar dryer and ambient air during experiments. The collector temperature followed a bell-shaped curve, peaking at 65–68 °C around solar noon, while the drying chamber reached 52–54 °C, consistently 15–20 °C lower due to heat transfer dynamics. Ambient temperatures ranged from 18 °C in the morning to 27–28 °C in the afternoon. The substantial temperature difference ($\Delta T \approx 25$–27 °C) highlights the system's effective solar energy capture, supporting accelerated drying.

Fig. 8 compares relative humidity (RH) profiles under ambient, conventional, and zeolite-enhanced drying conditions. Ambient RH decreased from 60–61 % in the morning to 38–39 % in the afternoon. Conventional drying started with 68.5 % RH, dropping to 29.6 % as drying progressed. Conventional drying started with 68.5 % RH and dropped to 44.8 % by the end of the experiment. In contrast, zeolite-enhanced drying achieved a lower final RH of 29.6 %, representing a 15 % absolute reduction. Additionally, the zeolite system reached a minimum RH of 16.8 % at the 4th hour. These results demonstrate zeolite's significant moisture adsorption capacity and its effectiveness in enhancing drying efficiency.

5.2. Drying kinetics

Fig. 9(a) shows the visual comparison of fresh samples and final dried product. Final dried products from control and zeolite-enhanced drying processes are shown Fig. 9(b). While both treatments achieved the target moisture content (10.37 % w.b.), no significant morphological differences were observed in terms of surface texture or shrinkage ratio. This suggests that zeolite's primary impact was kinetic (reducing drying time by 7.1 %) rather than qualitative under the tested conditions.

As in Fig. 10, it is seen that the zeolite-enhanced experiment achieved the target moisture content (10.37 % w.b.) 0.5 hours faster than the control experiment that demonstrates a 7.1 % reduction in total drying time. According to this figure, during the initial rapid drying phase (0–2 h), the zeolite-enhanced drying has an 18 % faster moisture removal rate, primarily due to the hygroscopic nature of zeolite. In the falling rate period (2–5 h), the zeolite-enhanced drying still maintained a 12 % advantage in the drying rate. Finally, in the approach to equilibrium (>5 h), the microporous structure of zeolite facilitated a more efficient drying process, enabling the sample to reach the target moisture content with potentially lower energy input. Consistent with the findings published by Dake et al. [3] the zeolite-enhanced drying consistently exhibited a lower moisture content throughout the entire process, underscoring the

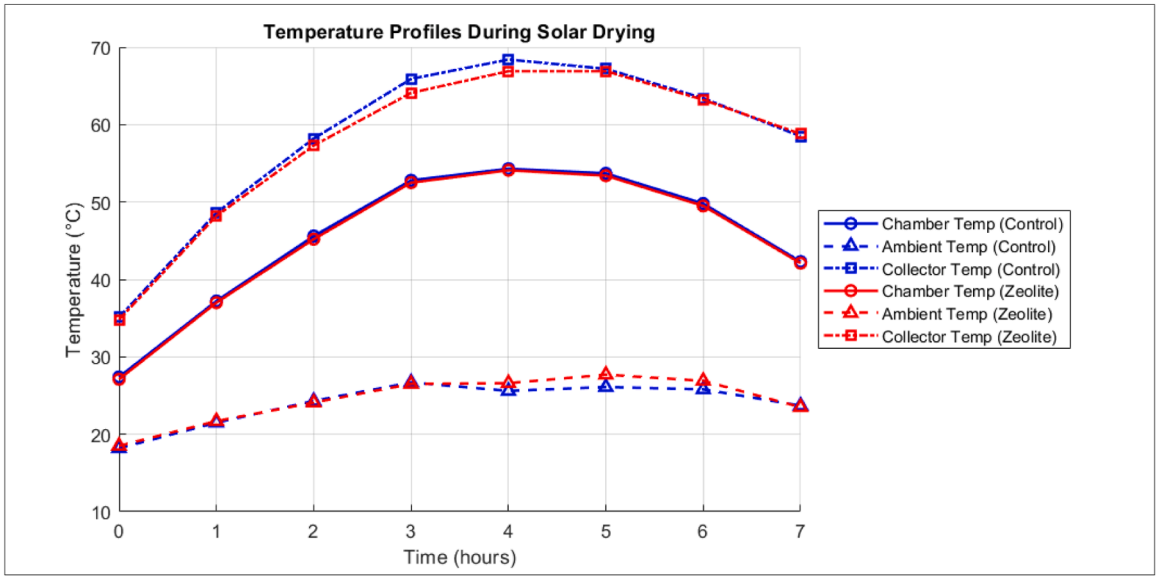

Fig. 7. Temperature profiles during solar drying experiments.

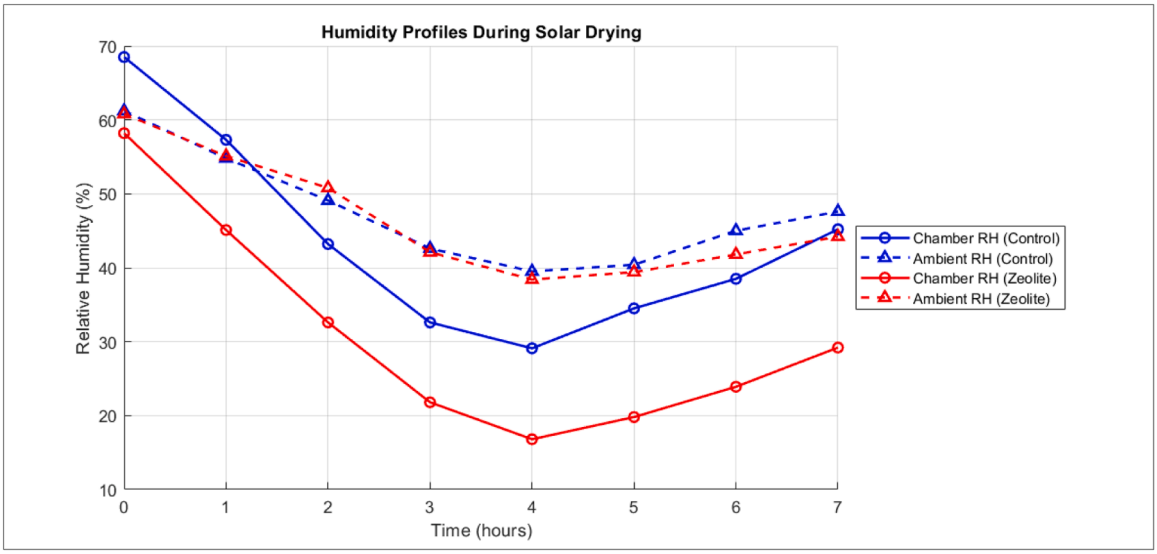

Fig. 8. Relative humidity profiles during solar drying experiments.

Fig. 9. (a) Fresh samples vs Final Dried Product (b) Final dried products: control(left), zeolite-enhanced (right).

effectiveness of zeolite in accelerating moisture removal and improving overall solar drying efficiency.

Fig. 11 illustrates the MR reduction over time for both control and zeolite-enhanced solar drying experiments. MR change reveals zeolite's significant enhancement of drying kinetics, achieving complete dehydration 0.5 hours faster than the control. The zeolite-enhanced curve exhibits steeper initial decline (MR reduction rate 32 % higher during 0–2 h), indicating that zeolite integration accelerates moisture removal. The faster decline in the moisture ratio with zeolite highlights its effectiveness in enhancing solar drying efficiency by facilitating moisture adsorption. Both systems transitioned to diffusion-dominated drying below MR = 0.4, though zeolite maintained 18 % faster rates until termination.

As presented in Fig. 12 the drying rate vs. moisture content profiles reveals three distinct drying regimes. In initial stage of drying (MC $>$ 2.5 g_w/g_{dm}), the zeolite-enhanced drying achieved a 42 % higher peak drying rate (1.24 vs. 0.87 $g_w/g_{dm}/h$), driven by strong vapor pressure gradient and zeolite's hygroscopic nature, which lower ambient humidity and accelerates evaporation.

Throughout the falling-rate period of drying (MC = 0.5–2.5 g_w/g_{dm}), the zeolite experiment demonstrated a significant acceleration in drying, with rates 28 % to 40 % higher than the control. This improves the ongoing dehumidification and exothermic heat release associated with moisture adsorption. In the final stage of drying (MC $<$ 0.5 g_w/g_{dm}), where internal diffusion dominates and drying slows, zeolite drying maintained a 71 % higher rate (0.12 vs. 0.07 $g_w/g_{dm}/h$), possibly due to stabilized thermal conditions and continued humidity control. This consistent enhancement through all drying phases demonstrates zeolite's high contribution to improving mass and heat transfer efficiency throughout drying process.

Although zeolite-enhanced drying exhibited higher drying rates throughout all phases, especially during the initial and falling-rate periods, the overall reduction in total drying time remained relatively modest (7.1 %). This is attributed to the dominance of internal moisture diffusion in the final stage of drying, which inherently slows down the process regardless of ambient conditions. While zeolite continued to improve drying rate even in this phase (71 % increase), its impact decreased as the product approached equilibrium moisture content. Therefore, the primary benefit of zeolite integration lies in accelerating the early high-moisture stages of drying, which helps reduce the duration of the most energy intensive segment.

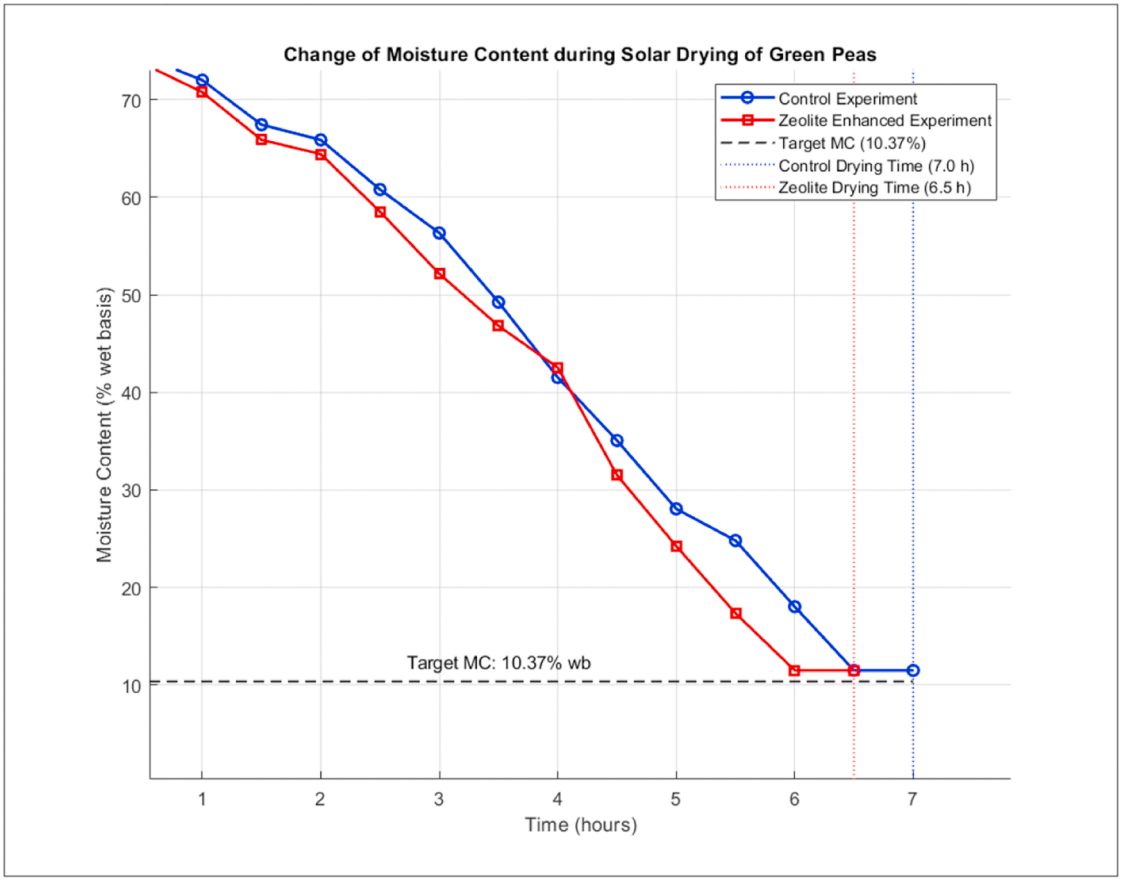

Fig. 10. Change of moisture content during solar drying experiments.

Table 7 summarizes the key energy performance metrics, comparing SMER and SEC values between control and zeolite-enhanced drying experiments. According to these results, zeolite-enhanced system demonstrated better energy performance, achieving a 4.6 % lower SEC (73.26 vs. 76.78 kWh/kg) and 5.4 % higher SMER (0.0137 vs. 0.013 kg/kWh) compared to the control experiment. This improvement supports the 7.1 % reduction in drying time (Fig. 10) and 32 % faster MR decline (Fig. 10), confirming zeolite's dual role in speeding the moisture removal while reducing specific energy demand. The energy savings are primarily from (i) enhanced heat/mass transfer during the rapid drying phase (42 % higher peak drying rate, as in Fig. 12), and (ii) maintained efficiency in falling-rate periods through zeolite's hygroscopic action [11,25]. Such findings are consistent with previous researches [9,33,34] highlighting the capacity of desiccant materials to improve the overall energy utilization efficiency of solar drying systems by accelerating the drying process.

5.3. *Zeolite performance*

In the zeolite-enhanced drying experiment, the moisture absorption of the zeolite (clinoptilolite) was measured by continuously observing its weight changes using load cells, and the hourly weight increase is plotted throughout the process as in Fig. 13. The difference in weight means the amount of vapor absorbed from the drying air. It absorbed approximately 92.6 g of moisture throughout the 6.5-hour drying period, representing an 1.85 % weight increase, summarized in Table 9. During the zeolite-enhanced drying experiment, the moisture absorption of clinoptilolite zeolite was continuously monitored using load cells, and the total weight gain was approximately 92.6 g (1.85 % increase), as shown in Table 8 and Fig. 13.

The moisture absorption profile followed a logarithmic trend, with the highest uptake occurring during the first 2 h, which corresponded to the period of most rapid moisture loss from the green peas as can be seen in Figs. 10 and 12. This temporal alignment result suggests that a portion of the evaporated moisture from the product was directly captured by the zeolite, thereby lowering the chamber's relative humidity and enhancing the drying environment.

However, it should be emphasized that while the parallel trends in drying rate and zeolite mass gain indicate a potential relationship, a direct causative correlation was not statistically quantified in this study. Future work may include a detailed correlation or regression analysis to rigorously examine the relationship between product moisture loss and zeolite absorption dynamics.

As shown in Fig. 13, the initial rapid moisture absorption (0-2 h) corresponds to the period of highest moisture removal from the

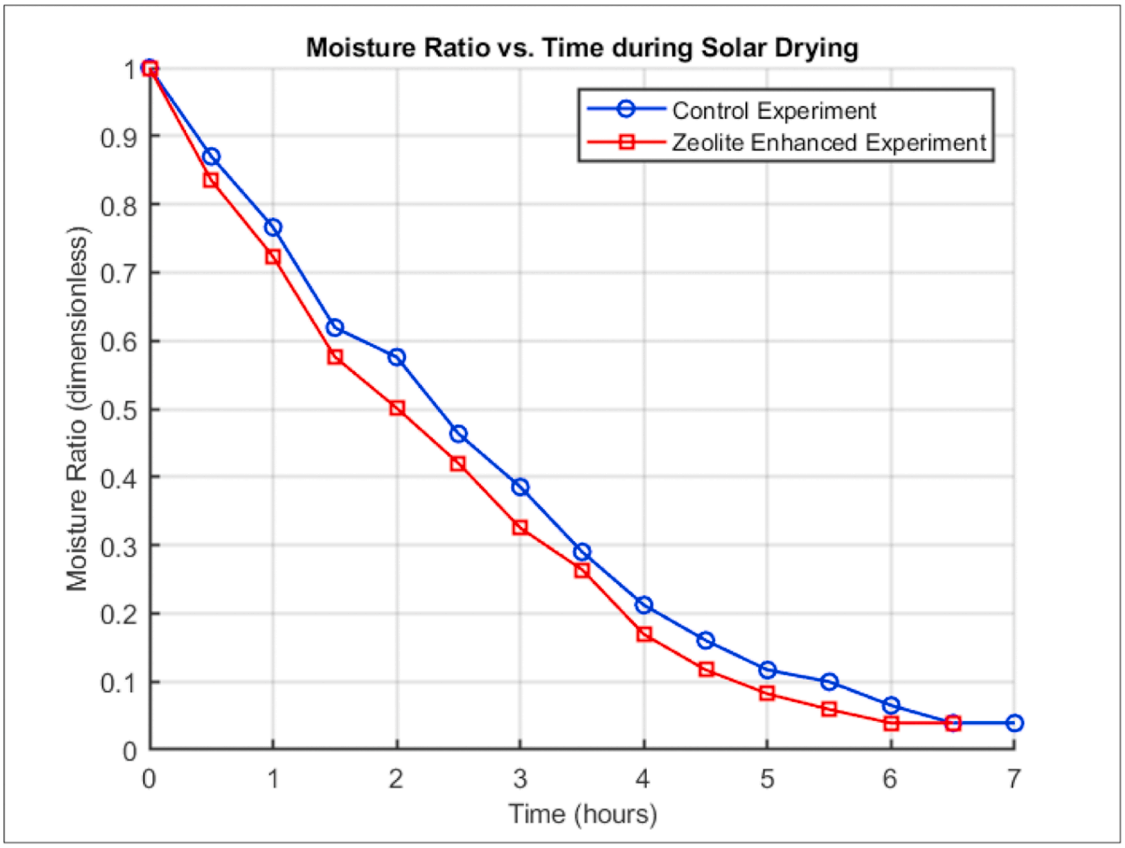

Fig. 11. Moisture ratio changes by time during solar drying.

green peas, where the greatest drying rate was observed. As expected, the moisture absorption rate of zeolite was initially high during the early hours of drying, corresponding with the highest product moisture release rate. This rate decreased over time as the product neared its equilibrium moisture content. The zeolite weight gain over time is expected to follow a decelerating growth trend.

Adsorption follows a logarithmic pattern, with higher absorption rates initially that diminish over time. The moisture absorption by zeolite is fitted a logarithmic function, and it is well-described by a logarithmic model of the form (Eq. 15):

$$W(t) = a\ln(bt+1) \tag{15}$$

where $W(t)$ is the cumulative weight increase of zeolite in percentage (%) at time t, t is the elapsed time in hours. This mathematical representation aligns with established adsorption theories for microporous materials like clinoptilolite zeolite [21]. The fitted parameters are found $a = 1.29$ and $b = 0.5542$. This model achieves an R^2 value of 0.9914, indicating a good fit to the theoretical data.

5.4. Mathematical modeling results

5.4.1. Control experiment results

The control drying experiment conducted on 15 April 2024 in Balıkesir required 7 hours (09:00–16:00) to reduce moisture content from 77 % to 10.37 % w.b., with half-hourly weight recordings via load cells. MR data were fitted to six thin-layer models using genetic algorithm optimization, with performance evaluated by R^2 and RMSE, presented in Table 9. The Karasu model achieved superior fit (R^2=0.9964, RMSE=0.0187), closely followed by the Midilli model (R^2=0.9962, RMSE=0.0193), as visualized in Fig. 14. Notably, these top models outperformed classical approaches (Page, Logarithmic) by >0.01 R^2 units, demonstrating their enhanced accuracy in predicting MR under suboptimal solar conditions characterized by 50.4 % lower irradiance than peak summer values.

5.4.2. Zeolite-enhanced experiment results

Conducted under nearly identical weather conditions on the 16 April 2024 the zeolite-enhanced drying achieved the target moisture content in 6.5 hours – a 7.1 % reduction in drying time compared to the control. The usage of zeolite significantly altered the drying kinetics, as reflected in the model parameters. The Karasu model demonstrated optimal fit (R^2=0.9968, RMSE=0.0174), with its moisture transfer coefficient k increasing by 19.9 % (0.2837 vs. 0.2367 in control), suggesting enhanced moisture diffusivity due to zeolite's hygroscopic action. Also, the shape parameter n decreased by 7.8 % (1.1597 vs. 1.2579), indicating a moderation of the

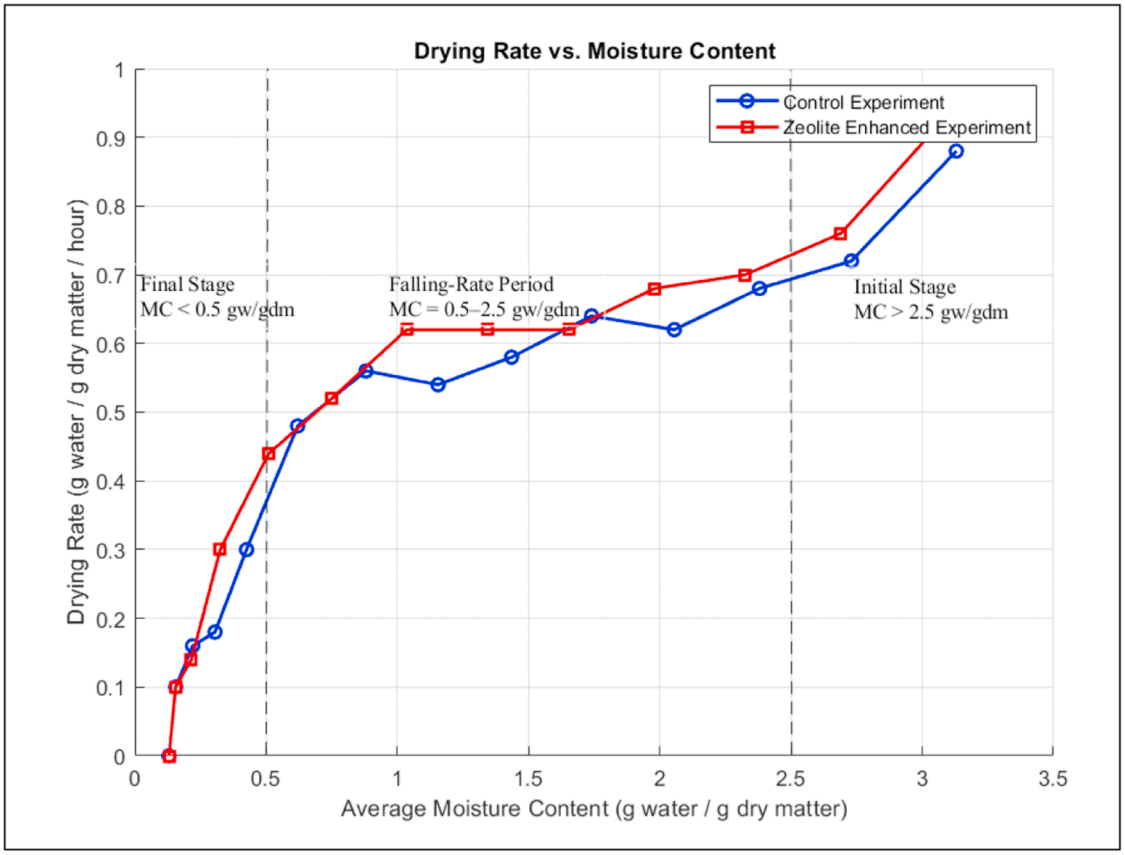

Fig. 12. Drying rate as a function of moisture content.

Table 7
Summary of energy performance metrics for drying experiments.

Performance Metric	Unit	Control Experiment (15th April)	Zeolite-Enhanced Experiment (16th April)
Fan Energy (E_{fan})	kWh	0.084	0.078
Solar Energy (E_{solar})	kWh	8.477	8.091
Total Supplied Energy ($E_{supplied}$)	kWh	8.561	8.169
Specific Moisture Extraction Rate (SMER)	kg/kWh	0.013	0.0137
Specific Energy Consumption (SEC)	kWh/kg	76.78	73.26

drying rate's time dependency, likely from zeolite's buffering effect on air humidity. The Midilli model closely followed (R^2=0.9965), with its drying constant k rising 27.7 % (0.3228 vs. 0.2528), further evidencing zeolite's impact on early-stage moisture removal. These parametric shifts, quantified in Table 10, and comparison of experimental and predicted moisture ratio graphs are shown in Fig. 15.

5.4.3. *Sensitivity analysis for karasu model parameters*

The sensitivity analysis of the Karasu model as previously named New Model 1 in Karasu Asnaz's paper [35] ($\boldsymbol{MR} = \boldsymbol{a}\ \mathbf{exp}[-(\boldsymbol{kt})^{\boldsymbol{n}}] + \boldsymbol{c}$) may reveal some insights into parameter influence on model performance, as evidenced by RMSE response curves across tested parameter ranges as presented in Fig. 16. The analysis demonstrates distinct behavioral patterns for each parameter.

- *Shape parameter n* exhibits the steepest RMSE curve slope, indicating that minor deviations from its optimal value cause significant prediction errors (>50 % RMSE increase). This confirms its dominant role in controlling the time-dependent drying rate profile.
- *Amplitude coefficient a*, controls the initial moisture ratio amplitude and it displays a sharp V-shaped error profile, where even ±0.05 variations from its optimum rapidly decrease the model performance.
- *Drying rate constant k* demonstrates a shallower slope, suggesting relative model robustness to its variations within ±0.2 range.
- *Offset parameter c* shows the flattest response, with RMSE changes remaining below 10 % across tested values.

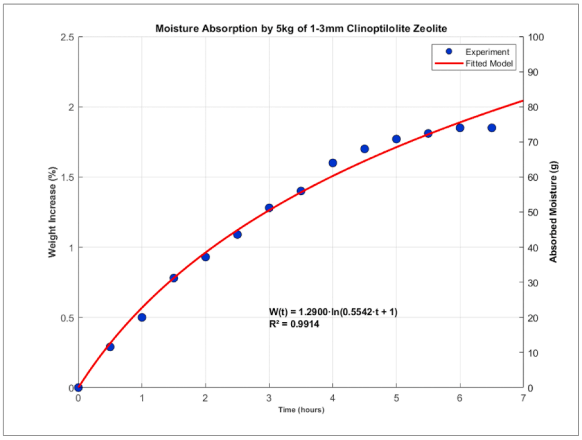

Fig. 13. The moisture absorption of zeolite and weight increase rate.

Table 8
Zeolite moisture absorption performance.

Parameter	Initial Zeolite Mass	Measurement Duration	Final Weight Increase	Total Moisture Absorbed	Absorption Capacity
Value	5 kg	6.5 h	1.85 %	92.5 g	18.5 $g_{water}/kg_{zeolite}$

Table 9
Summary results of each model (15th April, 2024 Control Experiment).

Model	a	k	n	b	c	RMSE	R2
Karasu Model *	1.0222	0.2367	1.2579	-	-0.0359	**0.0187**	**0.9964**
Midilli Model	0.9918	0.2528	1.2346	-0.0028	-	0.0193	0.9962
Page Model	-	0.2471	1.3036	-	-	0.0207	0.9956
Logarithmic Model	1.0612	0.375	-	-	0	0.0422	0.9817
Diffusion Model	0.4465	0.3576	-	0.9837	-	0.0473	0.9769
Lewis Model	-	0.354	-	-	-	0.0473	0.9769

The Karasu model proposed in this study introduces a structural refinement over the widely used Midilli model by replacing the linear term (bt), which can result in negative moisture ratio predictions during extended drying durations, with a constant parameter (c). In the Midilli model, the linear term bt may cause the MR to decrease below zero over time, producing physically unrealistic results in the final stages of drying. By replacing bt with a constant c, the Karasu model avoids this issue that ensures MR remains positive and asymptotically approaches a realistic equilibrium moisture content. In addition to this theoretical improvement, unlike simpler two-parameter models, it retains physical interpretability while accurately capturing nonlinear drying dynamics through four meaningful parameters (a, k, n, c), making it a reliable tool for solar drying analysis under varying environmental conditions.

5.5. Practical implications and insights

The findings of this study indicate that zeolite-enhanced thin-layer solar drying offers many advantages in terms of energy efficiency, product quality, and drying time under variable environmental conditions. Such systems can be integrated into small and medium scale agricultural applications with minimum requirements. Given that clinoptilolite zeolite is naturally abundant, non-toxic, and inexpensive, it provides a viable solution for decentralized food processing in rural or off-grid regions, where energy access and postharvest losses remain critical issues [9,25].

In addition to the benefits provided by zeolite, the proposed Karasu drying model offers a practical value for process simulation and control. The model demonstrates improved physical consistency and higher prediction accuracy compared to conventional empirical models, makes it suitable for real-time monitoring, and optimization of solar drying operations under variable environmental conditions.

To assess the economic feasibility of the proposed design, an initial cost analysis was conducted using the experimental parameters. In our setup, 5 kg of natural zeolite was applied over 0.5 m^2 of drying surface, corresponding to 10 kg/m^2. Based on a unit price of \$0.5/kg, the zeolite acquisition cost reaches \$5.00/m^2. Regarding regeneration, literature reports an average thermal energy demand of 0.8 MJ/kg for clinoptilolite [26] leading to a total of 8.0 MJ/m^2 in this study. Regeneration cost remains minimal when solar thermal energy is employed. A thermal energy cost of approximately \$0.01/MJ was assumed based on typical solar thermal systems, as reported by Fudholi et al. [36] resulting in an estimated regeneration cost of \$0.08/m^2. Additionally, clinoptilolite zeolite has been

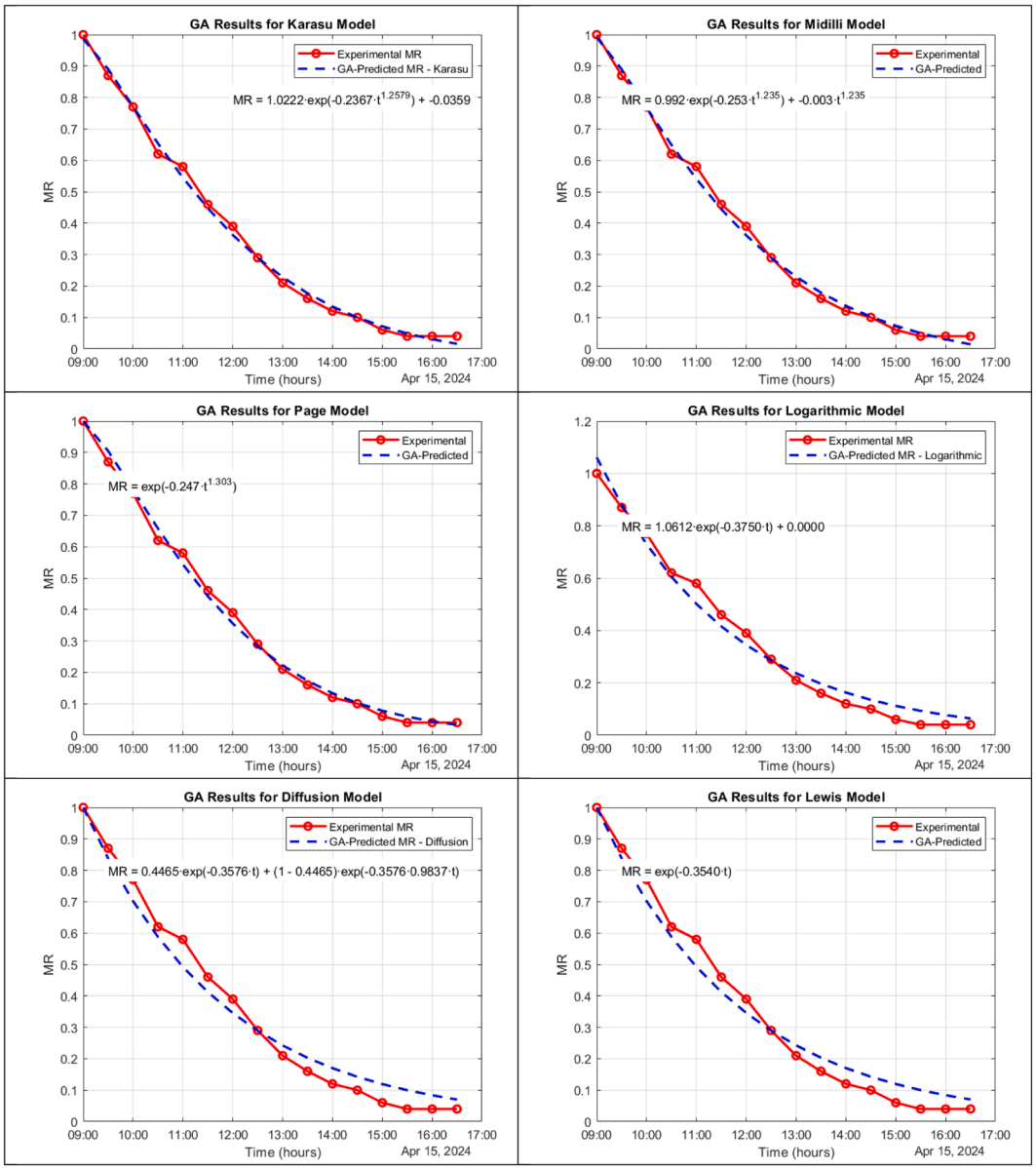

Fig. 14. Performance evaluation of six thin-layer drying models for control experiments (15 April 2024) Models ranked from best to worst fitting performance, with the Karasu model showing optimal agreement ($R^2 = 0.9964$, RMSE = 0.0187).

Table 10
Summary results of each model (16th April, 2024 Zeolite-Enhanced Experiment).

Model	a	k	n	b	c	RMSE	R2
Karasu Model *	1.05	0.2837	1.1597	-	-0.0684	**0.0174**	**0.9968**
Midilli Model	0.9999	0.3228	1.0587	-0.0125	-	0.0181	0.9965
Page Model	-	0.3112	1.2277	-	-	0.0232	0.9943
Logarithmic Model	1.0409	0.4135	-	-	0.0001	0.0376	0.9849
Diffusion Model	0	0.3431	-	1.1584	-	0.0404	0.9826
Lewis Model	-	0.3974	-	-	-	0.0404	0.9826

shown to maintain performance over multiple drying cycles and can be regenerated through solar energy without high temperature processing [37,38].

Some limitations should be acknowledged. The efficiency of zeolite regeneration can vary depending on ambient conditions such as

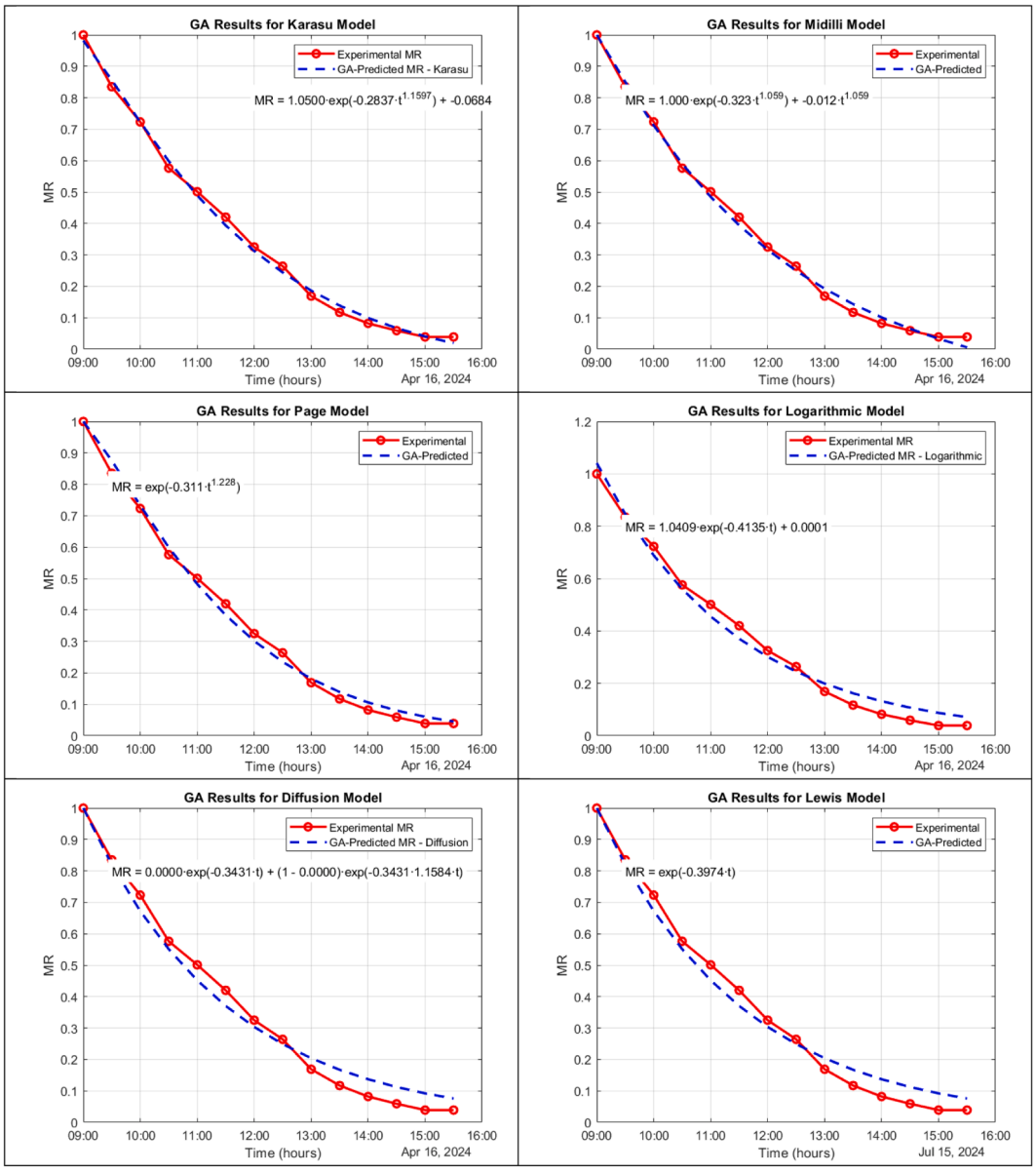

Fig. 15. Performance evaluation of six thin-layer drying models for zeolite-enhanced experiments (16 April 2024) Models ranked from best to worst fitting performance, with the Karasu model showing optimal agreement ($R^2 = 0.9968$, RMSE = 0.0174).

humidity and solar intensity. Additionally, potential contamination risks, particularly from repeated exposure to organic material, may necessitate periodic quality assessment or partial replacement of the zeolite layer [7,8]. Nevertheless, the integration of zeolite materials into solar drying systems improves drying time and contributes to food preservation capacity with minimal environmental and economic burden, thereby supporting sustainable development goals in the agricultural sector [10,25].

6. Conclusion

This study investigated the improvement of thin-layer solar drying of green peas using clinoptilolite zeolite under a high humidity and low solar radiation weather conditions in Balıkesir, Turkey. The research examined the impact of zeolite usage on drying kinetics, developed and validated mathematical models for predicting moisture ratio, and quantified the moisture absorption capacity of zeolite under solar drying conditions. The findings demonstrate that zeolite-enhanced solar drying offers a promising approach to overcome the limitations of conventional solar drying systems during periods of suboptimal weather conditions.

The key findings of this study can be summarized as follows:

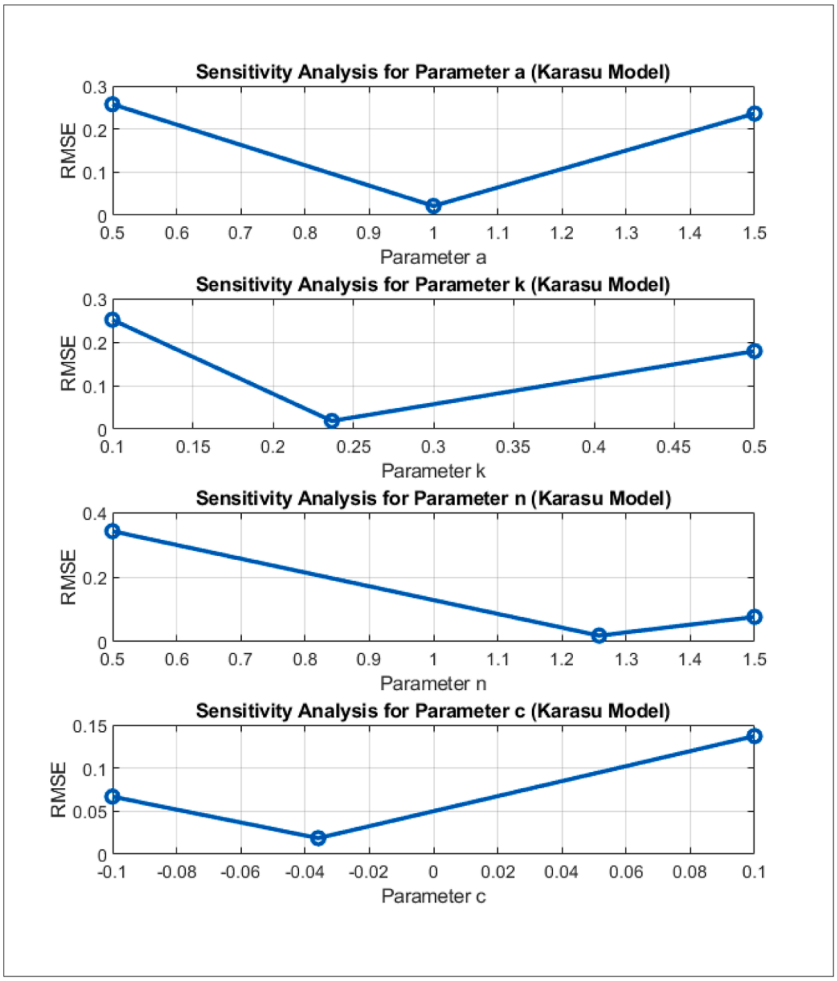

Fig. 16. Sensitivity analysis for parameters of Karasu Model.

- **Enhanced Drying Performance**: The integration of zeolite (1-3 mm particle size) reduced the total drying time by 7.1 % (from 7.0 to 6.5 hours) compared to conventional solar drying, demonstrating the effectiveness of zeolite as a moisture-adsorbing agent even under challenging environmental conditions.
- **Improved Drying Kinetics**: Zeolite-enhanced drying achieved a 42 % higher peak drying rate (1.24 vs. 0.87 g_w/g_{dm}/h) in the high-moisture regime and maintained a 28-40 % advantage throughout the falling-rate period. Most notably, a 71 % improvement was observed during the critical final drying phase (<0.5 g_w/g_{dm}), which typically represents the most energy-intensive portion of the drying process. The 4.6 % SEC reduction and 5.4 % SMER improvement were achieved through zeolite's moisture-adsorption capability rather than increased energy input that correlates directly with the observed shorter drying time and higher drying rates.
- **Effective Humidity Reduction**: The zeolite-enhanced system maintained consistently lower relative humidity levels in the drying chamber (average 25.98 % vs. 28.71 % in the control), and achieved up to a 15 % absolute reduction in RH compared to conventional drying during peak drying periods. This demonstrates zeolite's effectiveness in creating a more favorable environment for moisture removal.
- **Mathematical Modeling**: The proposed Karasu Model demonstrated very good performance in describing the drying behavior, achieving the highest coefficient of determination ($R^2 = 0.9968$) and lowest root mean square error (RMSE = 0.0174) for the zeolite-enhanced experiment. This four-parameter model outperformed traditional models including Lewis, Page, and Logarithmic formulations.
- **Novel Sensitivity Analysis**: The sensitivity analysis revealed that the shape parameter *n* had the most significant influence on model accuracy, with even minor deviations from its optimal value causing substantial prediction errors (>50 % RMSE increase). This finding represents a novel contribution to the field, as comprehensive sensitivity analyses are rarely conducted in drying kinetics studies.

- **Zeolite Moisture Absorption Performance**: The 5 kg of clinoptilolite zeolite absorbed approximately 92.6 g of moisture throughout the 6.5-hour drying period, representing an absorption capacity of 18.5 $g_w/kg_{zeolite}$. The moisture absorption pattern followed a logarithmic model with excellent fit ($R^2 = 0.9914$).
- **Quantified Parameter Influence**: The genetic algorithm optimization of model parameters revealed significant shifts in drying kinetics between conventional and zeolite-enhanced drying. The moisture transfer coefficient k increased by 19.9 % (0.2837 vs. 0.2367) in the zeolite experiment, indicating enhanced moisture diffusivity, while the shape parameter n decreased by 7.8 % (1.1597 vs. 1.2579), suggesting a moderation of the drying rate's time dependency due to zeolite's effect on air humidity in the drying chamber.

These findings demonstrate that zeolite integration offers a practical and effective approach to enhancing solar drying performance under challenging environmental conditions. A mathematical model developed in this study that provides a good tool for predicting and optimizing the drying behavior of agricultural products in zeolite-enhanced solar drying systems. However, it is important to note that in future studies, replicating the experiments under controlled environmental conditions or using climate chambers would provide further statistical confidence. However, this study offers valuable first-hand evidence of zeolite-enhanced drying performance in real-world, naturally fluctuating spring weather conditions. While the cost estimates provided in Section 5.5 offers a useful benchmark, they are based on specific experimental conditions and assumptions [25,36,37]. In real-world implementations, variations in zeolite market prices, regeneration efficiency under different climatic conditions, and operational factors such as maintenance and contamination risks may affect the overall feasibility.

Despite the benefits of zeolite-enhanced solar drying, several limitations must be acknowledged. The performance of clinoptilolite zeolite can be affected by ambient conditions, especially relative humidity and solar irradiance, that influence both drying and regeneration effectiveness. Additionally, natural zeolites may contain impurities and heavy metals and could pose contamination risks if not properly pre-treated or periodically assessed [7,8]. Over time, repeated exposures may weaken adsorption capacity, requiring partial replacement or thermal regeneration at an energy cost [3]. In addition to these limitations, mathematical modeling constraint should also be acknowledged. The proposed Karasu model, while offering improved empirical fit, is inherently data-driven and lacks a direct physical moisture transport foundation. Its performance is validated only under specific experimental conditions, limiting its generalizability across seasons or regions.

Future research could focus on several important directions. First, the optimization of zeolite quantity and particle size should be investigated to maximize drying efficiency while minimizing material costs. Second, comprehensive studies are needed to evaluate the potential impacts of zeolite proximity on food safety and the nutritional quality of dried products. Third, a comprehensive energy and exergy analysis is recommended to further evaluate the thermodynamic performance of the system and identify potential areas for efficiency improvement. Finally, validating the Karasu model under diverse conditions and against diffusion-based models would strengthen its applicability.

Artificial intelligence disclosure

During the preparation of this work, the author(s) used *DeepL* in order to assist with language translation and phrasing. After using this tool, the author(s) reviewed and edited the content as needed and take(s) full responsibility for the content of the publication.

Data availability

Data will be made available on request.

References

[1] O. Nnamchi, et al., Green Energy and Resources Solar dryers : A review of mechanism, methods and critical analysis of transport models applicable in solar drying of product, Green Energy Resour 3 (2) (2025) 100118.
[2] M.A. Kherrafi, et al., Advancements in solar drying technologies: design variations, hybrid systems, storage materials and numerical analysis: A review, Sol. Energy 270 (2024) 112383. Mar.
[3] R.A. Dake, K.E. N'Tsoukpoe, F. Kuznik, B. Lèye, I.W.K. Ouédraogo, A review on the use of sorption materials in solar dryers, Renew. Energy 175 (2021) 965–979.
[4] D.V.N. Lakshmi, P. Muthukumar, A. Layek, P.K. Nayak, Drying kinetics and quality analysis of black turmeric (Curcuma caesia) drying in a mixed mode forced convection solar dryer integrated with thermal energy storage, Renew. Energy 120 (2018) 23–34.
[5] A. Motevali, S. Minaei, A. Banakar, B. Ghobadian, M.H. Khoshtaghaza, Comparison of energy parameters in various dryers, Energy Convers. Manage. 87 (2014) 711–725.
[6] İ. Doymaz, N. Acaralı, Pea grains in drying: unraveling the kinetics of hot-air drying and exploring mathematical models for moisture diffusion, Isı Bilim. ve Tek. Derg. 44 (1) (2024) 217–226.
[7] V. Kochubei, S. Yaholnyk, M. Malovanyy, N. Buchaichuk, Study of the influence of dispersion and conditions of thermal activation on the sorption properties of transcarpathian clinoptilolite and prospects for its application in environmental technologies, Environ. Probl. 9 (4) (2024) 218–226.
[8] M. Djaeni, L. Kurniasari, S.B. Sasongko, Preparation of natural zeolite for air dehumidification in food drying, Int. J. Sci. Eng. 8 (April) (2015) 80–83.
[9] T. Ying, A. Dien, K. Kornbluth, C.W. Simmons, I.R. Donis-González, E.S. Spang, Energy performance of zeolite-based drying bead desiccants used to dry paddy rice, ACS. Omega 9 (36) (2024) 38142–38152.
[10] Z.D. Siqhny, A.R. Sari, F.D. Utari, M. Djaeni, Drying kinetics and thermal energy evaluation of moringa oleifera leaves drying using dehumidification with zeolite, J. Bioresour. Environ. Sci. 3 (1) (2024) 53–60.
[11] F.D. Utari, M. Djaeni, F. Irfandy, Constant rate of paddy rice drying using air dehumidification with zeolite, IOP. Conf. Ser. Earth. Environ. Sci. 102 (1) (2018).
[12] L. Buchori, M. Djaeni, L. Kurniasari, The effort of efficiency and quality improvement on corn drying process using mixed-adsorption dryer, Reaktor 14 (3) (2013) 193.

[13] K.A. Metwally, et al., The mathematical modeling, diffusivity, energy, and enviro-economic analysis (MD3E) of an automatic solar dryer for drying date fruits, Sustain 16 (8) (2024).
[14] J. Haydary, M.J. Royen, A.W. Noori, Process conditions sensitive (PCS) thin-layer mathematical model of hot air convective drying, Chem. Eng. Commun. 211 (1) (2024) 133–145.
[15] K. Sherazi, N. Sheikh, M. Anjum, A.G. Raza, Solar drying experimental research and mathematical modelling of wild mint and peach moisture content, J. Asian Sci. Res. 13 (2) (2023) 94–107.
[16] T.K. Abdelkader, et al., Machine learning, mathematical modeling and 4E (energy, exergy, environmental, and economic) analysis of an indirect solar dryer for drying sweet potato, Renew. Energy 227 (2024) 120535. Jun.
[17] M. Peter, et al., Computational intelligence and mathematical modelling in chanterelle mushrooms' drying process under heat pump dryer, Biosyst. Eng. 212 (2021) 143–159.
[18] X. Wang, R. Xue, P. Gong, B. Wang, W. Hao, L. Wang, Drying characteristics, sustainability assessment and machine learning predictions of glass greenhouse drying system with photovoltaic roof, Case Stud. Therm. Eng. 69 (2025) 106044.
[19] B. Takgil, R. Kara, Proposing a novel mathematical model for hospital pneumatic system, Int. J. Optim. Control Theor. Appl. 14 (2) (2024) 113–122.
[20] A. Zoukit, H. El Ferouali, I. Salhi, S. Doubabi, N. Abdenouri, Takagi Sugeno fuzzy modeling applied to an indirect solar dryer operated in both natural and forced convection, Renew. Energy 133 (2019) 849–860. Apr.
[21] M. Beigi, M. Tohidi, M. Torki-Harchegani, Exergetic analysis of deep-bed drying of rough rice in a convective dryer, Energy 140 (2017) 374–382. Dec.
[22] M.S. Karasu Asnaz, A.O. Dolcek, Comparative performance study of different types of solar dryers towards sustainable agriculture, Energy Reports 7 (2021) 6107–6118.
[23] "JRC Photovoltaic Geographical Information System (PVGIS) - European Commission." [Online]. Available: https://re.jrc.ec.europa.eu/pvg_tools/en/#PVP. [Accessed: 18-Jan-2025].
[24] A. Motevali, S. Minaei, A. Banakar, B. Ghobadian, M.H. Khoshtaghaza, Comparison of energy parameters in various dryers, Energy Convers. Manage 87 (2014) 711–725. Nov.
[25] P.J. Nassari, D.M. Lwabulala, M.S. Ngomuo, A.K. Theophil, Evaluation of desiccants zeolite beads technology for drying four seed crops (Green Gram-Vigna Radiata L., Onion-Allium Cepa L., Amaranthus L., Tomato- Lycoperscon Esculentum L.) and their effect on seed storability and quality, Int. J. Agric. Environ. Res. 10 (02) (2024) 274–286.
[26] N. Widiastuti, H. Wu, H.M. Ang, D. Zhang, Removal of ammonium from greywater using natural zeolite, Desalination. 277 (1–3) (2011) 15–23.
[27] M.S. Karasu Asnaz, New mathematical models of thin layer solar drying of carrots, J. Sci. Ind. Res. 81 (2022) 21–31.
[28] K. Venkateswarlu, S.V.K. Reddy, Recent trends on energy-efficient solar dryers for food and agricultural products drying: a review, Waste Dispos. Sustain. Energy 6 (3) (2024) 335–353.
[29] T. Rubina, A. Aboltins, J. Palabinskis, E. Jotautiene, Study of drying and rehydration kinetics of carrot cylinders, Eng. Rural Dev. 17 (2018) 1488–1493.
[30] A.K. Karthikeyan, S. Murugavelh, Thin layer drying kinetics and exergy analysis of turmeric (Curcuma longa) in a mixed mode forced convection solar tunnel dryer, Renew. Energy 128 (2018) 305–312.
[31] M. Gulsen, A.E. Smith, D.M. Tate, A genetic algorithm curve fitting, Int. J. Prod. Res. 33 (7) (1995) 1911–1923.
[32] M. Kaya, O. Ozkan, UAV routing with genetic algorithm based matheuristic for border security missions, Int. J. Optim. Control Theor. Appl. 11 (2) (2021) 128–138.
[33] V. Shanmugam, E. Natarajan, Experimental investigation of forced convection and desiccant integrated solar dryer, Renew. Energy 31 (8) (2006) 1239–1251.
[34] S. Misha, S. Mat, M.H. Ruslan, E. Salleh, K. Sopian, Performance of a solar assisted solid desiccant dryer for kenaf core fiber drying under low solar radiation, Sol. Energy 112 (2015) 194–204. Feb.
[35] M.S. Karasu Asnaz, New mathematical models of thin layer solar drying of carrots, J. Sci. Ind. Res. (India) 81 (1) (2022) 21–31.
[36] A. Fudholi, K. Sopian, M.Y. Othman, M.H. Ruslan, Energy and exergy analyses of solar drying system of red seaweed, Energy Build. 68 (PARTA) (2014) 121–129.
[37] D. Bariho, W. Kisaalita, L. Kasisira, Solar energy zeolite regeneration for a milk cooler, J. Agric. Mach. Sci. 4 (3) (2008) 265–268.
[38] F.A. Mumpton, La roca magica: uses of natural zeolites in agriculture and industry, Proc. Natl. Acad. Sci. u S. a 96 (7) (1999) 3463–3470.